Available online at www.sciencedirect.com
ScienceDirect
Journal of the European Ceramic Society 31 (2011) 723–731
www.elsevier.com/locate/jeurceramsoc

Growth mechanism of single-crystal α-Al_2O_3 nanofibers fabricated by electrospinning techniques

Pei-Ching Yu [a], Rung-Je Yang [a], Yi-Yang Tsai [b], Wolfgang Sigmund [b,c], Fu-Su Yen [a,*]

[a] Department of Resources Engineering, National Cheng Kung University, No. 1 University Road, Tainan 70101, Taiwan, ROC
[b] Department of Materials Science and Engineering, University of Florida, Gainesville, FL 32611-6400, USA
[c] WCU Energy Department, Hanyang University, Seoul, South Korea

Received 1 April 2010; received in revised form 2 November 2010; accepted 21 November 2010
Available online 17 December 2010

Abstract

Crystal-growth-related microstructures and the length-to-diameter ratio of a single-crystal-type α-Al_2O_3 nanofiber were examined using HR-TEM techniques. The fibers exhibited diameters ranging from 50 to 100 nm and lengths of several tens of micrometers. During thermal treatments, the alumina fiber went through phase transformations similar to boehmite. Therefore, the phase evolution, especially the final θ- to α-Al_2O_3 stage of the phase transformation, may be the determining factor in the microstructural evolution of the nanofibers. HR-TEM techniques were utilized to demonstrate that the single crystals were formed by the coalescence of well-elongated α-Al_2O_3 colonies. The fibers grew in the [1 1 0] or [1 1 2] direction instead of [0 0 1]. A thermodynamic analysis revealed that if the α-Al_2O_3 nanofiber that transformed from θ-Al_2O_3 behaved in a stable manner, there could be a size ratio limit for the length and diameter of each α-Al_2O_3 colony. The smallest potential diameter was calculated to be around 17 nm.

Keywords: Al_2O_3; Fibers; Calcination; Electrospinning

1. Introduction

The technology used to manufacture continuous high-alumina fibers at the mass production scale was developed in 1963.[1] This polycrystalline fiber has mainly been used in the refractory industry. The dimensions of these types of fibers were micrometers in diameter and centimeters in length. Two processes, denoted as the slurry and solution (or sol–gel) processes, have been developed to produce these alumina fibers.[2] These techniques differ in the methods utilized to prepare precursors. The former uses an aqueous suspension of Al_2O_3 particles, while the latter uses solutions of aluminum[3–6] or organoaluminum[7] compounds. The subsequent processes in these two techniques are more or less the same; these include the extrusion and drawing of slurries or solutions, followed by drying and a final heat treatment at high temperatures for the fibers. Normally, α-Al_2O_3 fibers are obtained through a sequence of phase transformations (i.e., non-crystalline/amorphous $Al_2O_3 \rightarrow$ γ- $\rightarrow$ δ- $\rightarrow$ θ- $\rightarrow$ α-Al_2O_3). Dissolved organic polymers are sometimes added to control the rheology (e.g., viscosity, stability of slurries or solutions) of the precursors to facilitate the formation processes.[2] The main advantages of these two processes are as follows: applicability in mass production; control of crystalline phases generated in the fibers via thermal treatment; determination of fiber chemical composition from starting materials; and no required catalysts or substrates for fiber growth. However, at this time, single-crystal α-Al_2O_3 fibers have not been fabricated in industry using these processes.

Single-crystal Al_2O_3 fibers were first produced in 1996.[8] This type of fiber is both thermally and chemically stable, in addition to having a higher elastic modulus as compared to polycrystalline fibers.[1] Therefore, these fibers are mainly used in the reinforcement of composite materials such as metal matrix composites (MMCs). Instead of the several-micrometer-sized diameters achieved for polycrystalline fibers, single-crystal fibers can be <100 nm in diameter and have lengths reaching

* Corresponding author. Tel.: +886 6 2355603; fax: +886 6 2380421.
E-mail address: yfs42041@mail.ncku.edu.tw (F.-S. Yen).

0955-2219/$ – see front matter © 2010 Elsevier Ltd. All rights reserved.
doi:10.1016/j.jeurceramsoc.2010.11.011

tens of micrometers. Several methods have been reported for the production of these types of fibers. However, such techniques usually involve processes that are assisted by catalysts or substrates, especially for methods that are conducted using models of tip growth and basal growth.[2] In 1996, Lawrence Berkeley National Laboratory (Berkeley, CA, USA) produced the first single-crystal Al_2O_3 fibers using the vapor–liquid–solid (VLS)[9] deposition technique, in which sapphire was used as the substrate and molten Pt droplets were introduced onto the substrate to act as catalysts.[8] Later approaches have adopted a so-called "displacement reaction" by heating mixtures of powder aluminum (Al) and metal oxides, such as SiO_2,[10–17] MoO_3,[17] WO_3,[17] or SiC[18] in an argon atmosphere to fabricate single-crystal fibers, whiskers, and nanowires. The growth of the fibers/whiskers was found to be mostly in the [0 0 1] direction through the VLS mechanism[10–15,18] or through a mechanism that is analogous to Ostwald ripening.[16,17] Both of these mechanisms are categorized as tip growth models, resulting in characteristic round droplets or slight sharp curvatures on the tips of the fibers/whiskers. A similar method (basal growth) of growing α-Al_2O_3 whiskers in an aluminum-based MMC has been reported using an internal oxidation reaction between aluminum and molybdenum oxide (MoO_3) at 850 °C.[19] The α-Al_2O_3 whiskers obtained were, on average, 1 μm in diameter and 10 μm in length. Similarly, the basal [0 0 1] growth model has been confirmed by energy dispersive spectrometer (EDS) and microstructure analyses. However, it is not easy to prepare these types of single-phase powders or to achieve a high chemical purity using the displacement reaction.

Electrospinning is another useful technique for the production of continuous polymeric and ceramic nanofibers.[20,21] This process normally consists of two steps, being similar to the conventional solution processes.[2] First, spun fibers composed of a ceramic precursor, polymer and solvent are obtained. Second, ceramic fibers are formed using appropriate thermal treatments. The first ceramic nanofibers prepared by this method were reported in 2002.[20,21] Since then, more than 20 varieties of ceramic fibers (e.g., SiO_2, ZrO_2, TiO_2, and Al_2O_3) have been produced.[20,22,23] Fibers formed using this method have been prepared with diameters of <100 nm. Most of these fibers are polycrystalline. There are few reports of single-crystal α-Al_2O_3 nanofibers fabricated by electrospinning. The first preparation of single-crystal α-Al_2O_3 nanofibers by electrospinning was reported in 2006.[24] Nevertheless, the growth mechanism of α-Al_2O_3 nanofibers has not been discussed.

The production of single-crystal α-Al_2O_3 nanofibers could be more economical if the nanofibers were obtained by methods similar to the current conventional means. Alternatively, it could be more practical to manufacture the nanofibers via the thermal treatment of fibrous precursors that are prepared by methods similar to those used in the manufacture of polycrystalline fibers. From this perspective, there are two crucial issues to be resolved: (1) the dimensions of the as-prepared fiber precursors should be controlled to certain sizes to result in Al_2O_3 fibers with diameters of <100 nm, and (2) the shape of the precursors must be maintained during subsequent thermal treatments. Of course, for the formation of a fiber crystallite, the basic thermodynamic requirements must be satisfied. At this point, the two issues are ready to be solved.

Table 1
Comparison of electrospinning conditions adopted in the reference and the current study.

Electrospinning conditions	Reference[24]	Current study
Needle size, gauge	23	16
Distance between needle and collector, cm	10	10
Flow rate, ml/h	0.03	0.9
Voltage, kV	7–9	9

This study focuses on the second issue listed above. Examinations of the crystal-growth-related microstructures and the thermodynamic-related size ratios (length-to-diameter) of α-Al_2O_3 nanofibers were performed using high-resolution transmission electron microscopy (HR-TEM). These analyses were aimed at formulating the growth mechanism of single-crystal-type α-Al_2O_3 nanofibers. First, we assumed that the nanofibers could be obtained using a two-step fabrication process. To fit this assumption, single-crystal α-Al_2O_3 nanofibers with diameters of <100 nm were prepared using the electrospinning technique.[20,21] Several previous reports[24,25] were utilized to select the appropriate fabrication conditions. To satisfy the thermodynamic requirements for nanofiber crystallite formation, the total free energy changes of the phase transformation (θ- to α-Al_2O_3 phase transformation[24,26]) were analyzed. The θ- to α-Al_2O_3 phase transformation is achieved by the nucleation and growth mechanism.[27–30] Thus, the thermodynamic stability of the crystallites is related to their volume and surface free energies.[26] Based on this, the diameter and length that make up the volume and surface of the nanofiber crystallites could presumably experience certain limitations. The length-to-diameter ratios of the nanofibers were briefly examined. Finally, the smallest nanofiber diameter was calculated.

2. Experimental

2.1. Fibrous precursor preparation

As-prepared fibrous precursors forming α-Al_2O_3 nanofibers were obtained by the electrospinning technique. The report by Azad[24] was used to guide the selection of the Al_2O_3 precursor, polymer and solvent. Aluminum 2,4-pentanedionate (AP; $Al(CH_3COCHCOCH_3)_3$; 99% purity; Alfa-Aesar, USA) dissolved in acetone (Fisher Chemicals, USA) was used as the precursor for the synthesis of alumina fibers. Granular polyvinyl pyrrolidone (PVP, average molecular weight ~1.3×10^6, Acros, USA) was used as the polymeric component and dissolved in ethanol (Acros, USA). For the experimental conditions, some parameters were modified from the reference (Table 1). During electrospinning, as-spun fibers were collected on a silicon wafer for observation under a scanning electron microscope (SEM). Fig. 1(a) displays the SEM micrographs of as-spun fibers, showing diameters in the range of 200–400 nm.

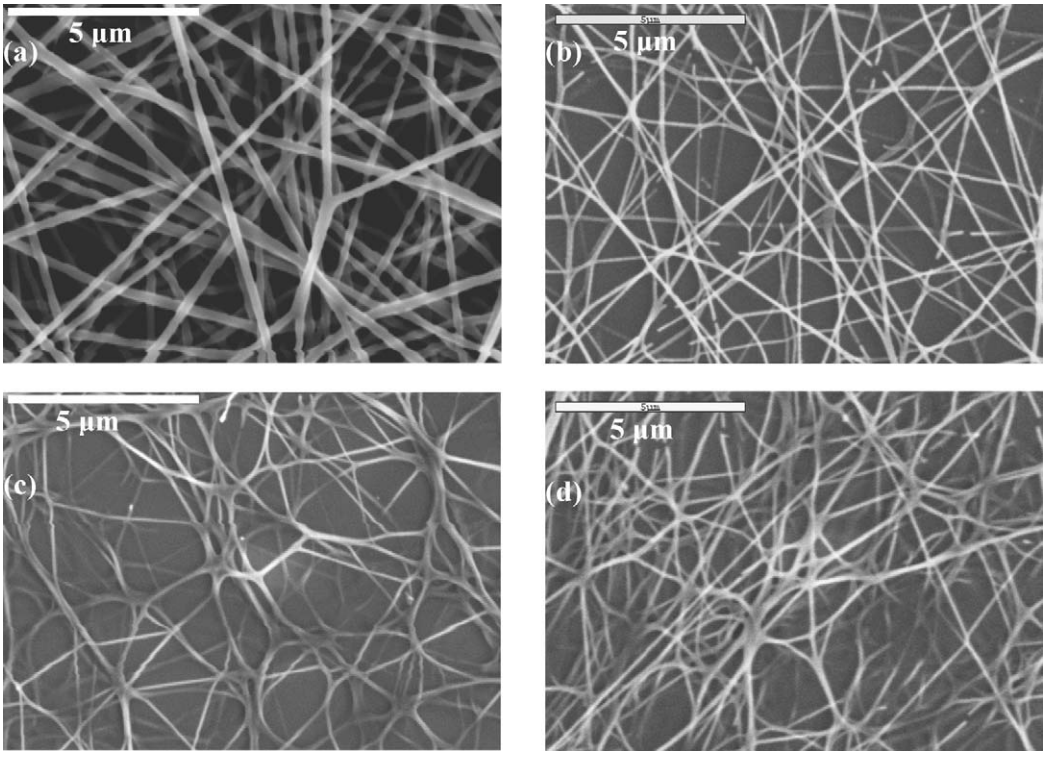

Fig. 1. SEM micrographs of as-spun fibers (a) and nanofibers calcined at 1000 °C (b), 1150 °C (c), and 1200 °C (d).

2.2. Thermal treatments

To obtain α-Al_2O_3 nanofibers, thermal treatment processes were performed in a tube furnace with flowing inert argon gas. Volatile organic matters usually experience incomplete combustion at lower temperatures. In this study, at temperatures <750 °C, flowing inert argon gas was adopted to carry most part of volatile matters out as well as preventing combustion of the organics which might destroy the fabricated morphologies of as-spun fibers. As temperature raised (>750 °C), the argon flow was gradually replaced by air as to remove the residual organic matters. It seems a complete burnout of organics can be achieved in this case. And Al_2O_3 fibers were fabricated at higher temperature without residue of carbon. As-spun fibers collected on a silicon wafer were placed in alumina crucibles and thermally treated to the programmed temperatures (800–1300 °C) at a heating rate of 10 °C/min. After the furnace was cooled, the calcined samples were collected for further characterization.

2.3. Characterization

The thermal behavior of as-spun fibers was examined by simultaneous differential thermal analysis (DTA/TG, Setaram TGA 92, Setaram Instrumentation, Caluire, France) using ignited alumina as the reference material. The heating rate was 10 °C/min, reaching a maximum temperature of 1450 °C. The crystalline phase was identified by XRD (Rigaku MiniFlex, Rigaku Corp., Tokyo, Japan) powder methods[31] using CuKα radiation ($2\theta = 20–80°$). The morphology and microstructures of the fibers were studied by scanning electron microscopy (SEM, JEOL SEM 6400) and transmission electron microscopy (TEM, Hitachi HF-2000; HR-TEM, FEI Tecnai F20). To prepare TEM samples, calcined samples were placed in ethanol, and ultrasonic treatment was utilized to form a suspension. A drop of the suspension was allowed to fall through a carbon-coated copper grid, leaving the powder on the grid for TEM examination.

3. Results and discussion

3.1. Fiber morphology

Fig. 1 displays SEM micrographs of as-spun fibers and the thermally treated α-Al_2O_3 nanofibers. As shown in the figure, individual as-spun fibers with identical morphological features were prepared, and they exhibited diameters in the range of 200–400 nm (Fig. 1(a)). The fibrous and continuous morphologies were well retained for the as-spun fibers, despite a significant decrease in diameter after thermal treatments.

3.2. Phase evolution analysis

The DTA profile of the as-spun fibers is presented in Fig. 2. A series of reactions, include dehydration, polyvinyl pyrrolidone (PVP) burnout, and decomposition of organic groups, from the organometallic precursor occurred sequentially prior to reaching 800 °C.[32] An exothermal peak appeared at around 1200 °C. This coincided with the temperature for the formation of α-

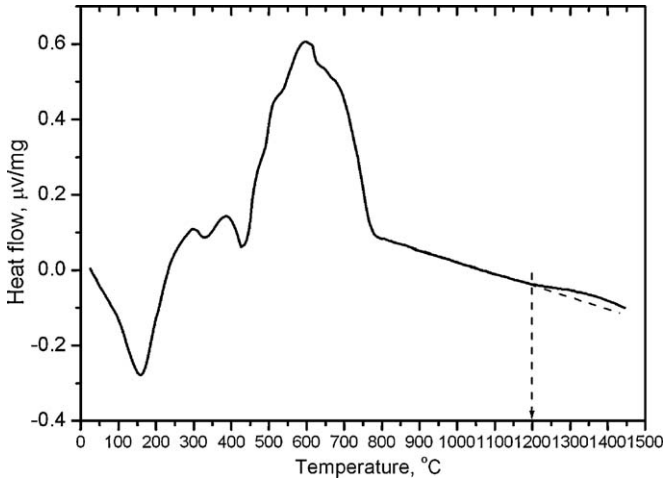

Fig. 2. DTA profile of the as-spun fibers with a heating rate of 10 °C/min. α-Al_2O_3 occurs at 1200 °C.

phase alumina, in general.[33] The corresponding XRD patterns for alumina phase identification are presented in Fig. 3. At 800 °C, the peaks are broad, revealing that the calcined fibers were amorphous/microcrystalline. As the thermal treatments progressed, γ-Al_2O_3 was the principal phase observed at 1000 and 1050 °C, although δ-Al_2O_3 was also identified. The peaks of α-Al_2O_3 appeared and γ-Al_2O_3 almost disappeared at 1100 °C. In the range of 1100–1200 °C, the nanofibers of δ-, θ-, and α-Al_2O_3 co-existed. Finally, at 1200 °C, the pure-phase α-Al_2O_3 fiber was the only phase present. From the above results, the phase evolution of alumina fibers in this study can be shown as follows:

Amorphous/microcrystalline→γ-Al_2O_3 → δ-Al_2O_3 → θ-Al_2O_3 → α-Al_2O_3.

This is the typical phase transformation route of boehmite to α-Al_2O_3.

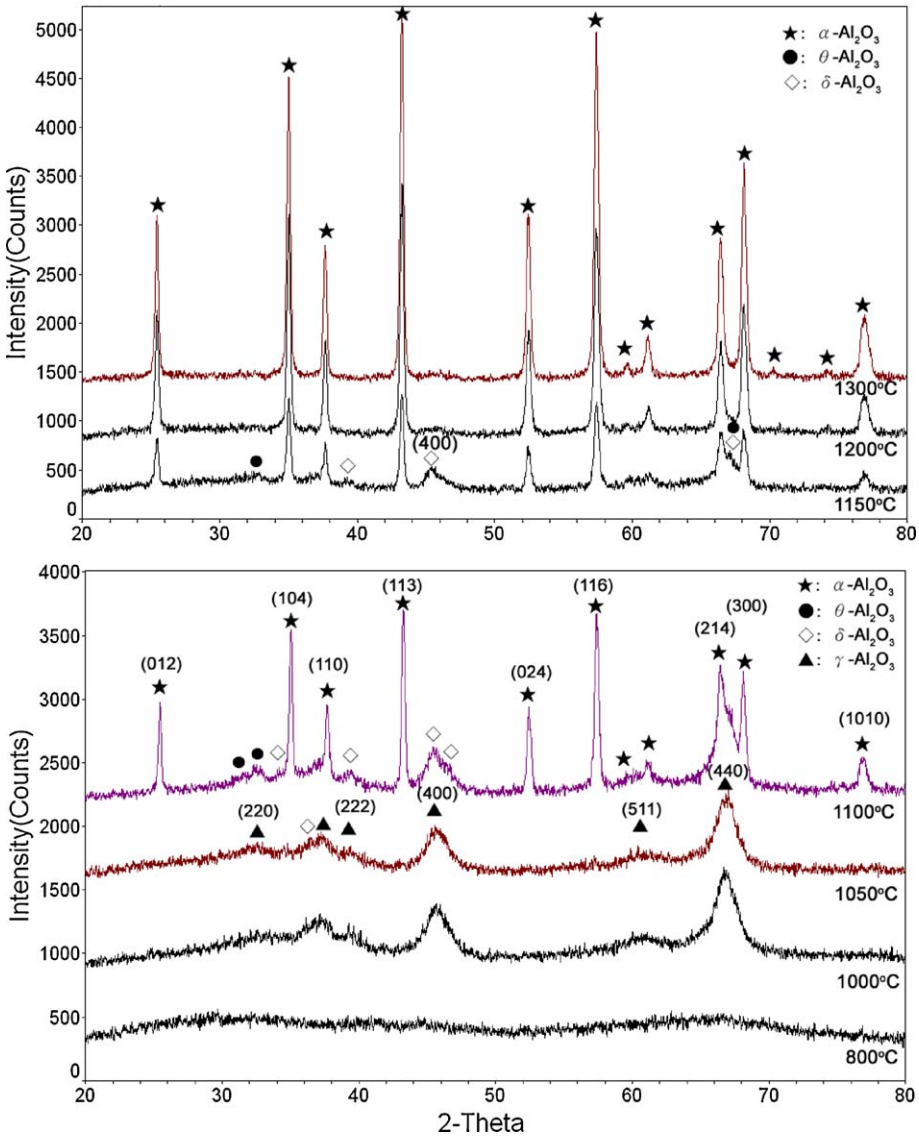

Fig. 3. XRD patterns of Al_2O_3 nanofibers calcined at temperatures of 800–1300 °C. The pure α-phase of the Al_2O_3 nanofibers was obtained at 1200 °C.

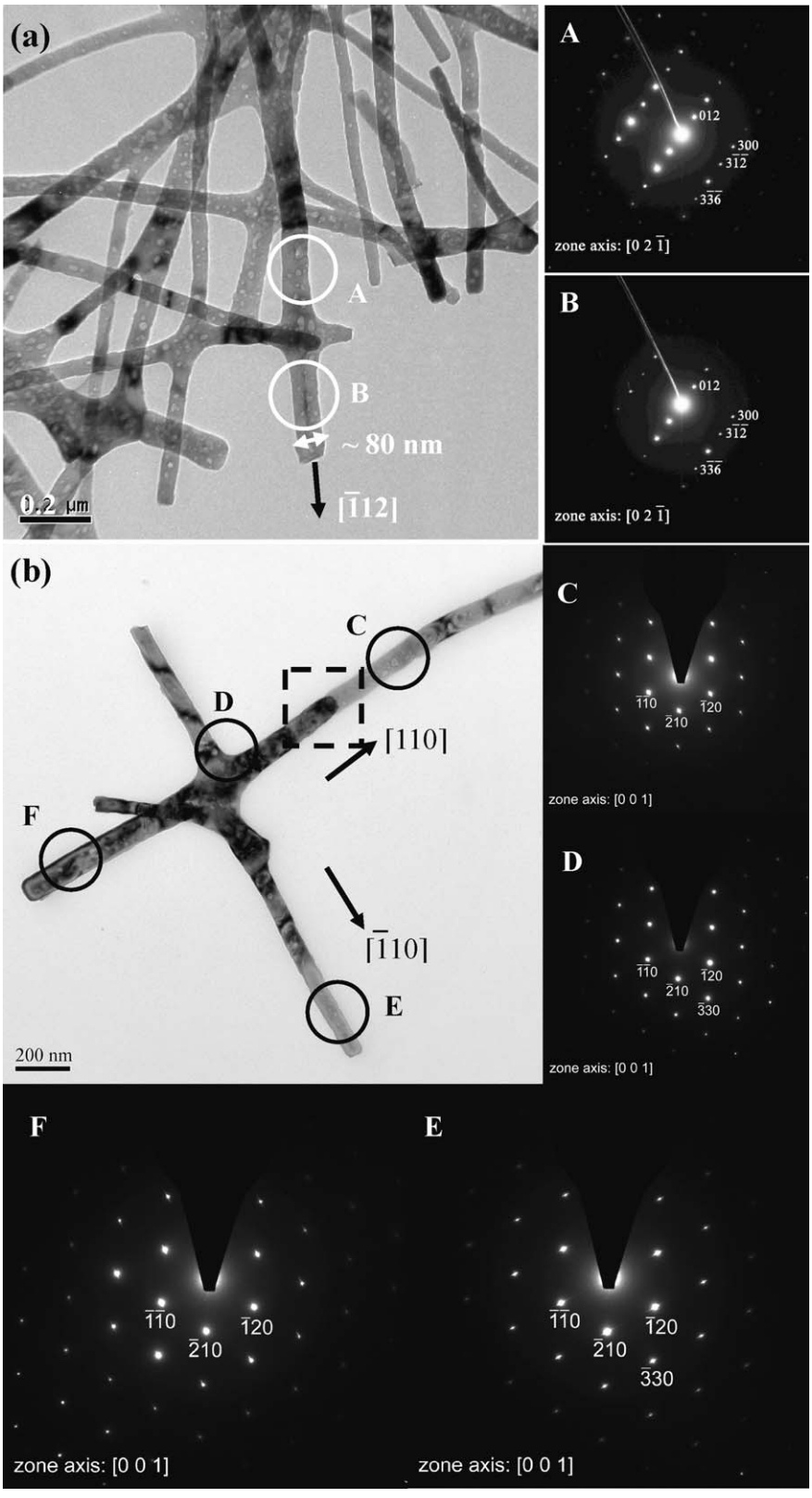

Fig. 4. TEM bright-field images and corresponding diffraction patterns of α-Al_2O_3 nanofibers calcined at 1200 °C, showing continuity with the electronic diffraction (ED) patterns and the elongation directions.

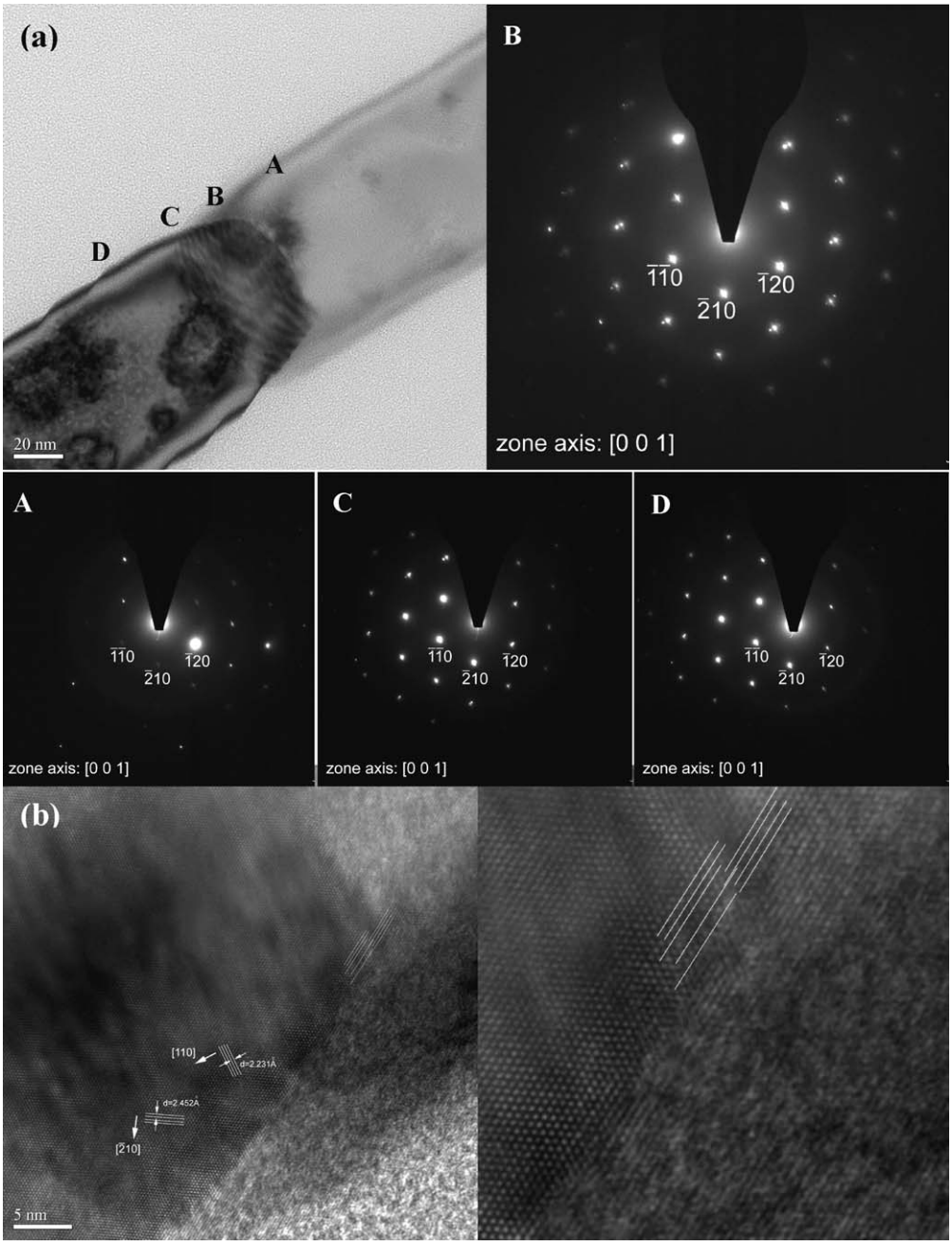

Fig. 5. ED patterns (a) and HR-TEM images (b) of the square area in Fig. 4(b). Some spots are separated in the ED pattern of region B, demonstrating the low-angle grain boundary that resulted from the coalescence of well-elongated α-Al_2O_3 fibers.

3.3. Single-crystal alumina nanofibers

α-Al_2O_3 nanofibers were formed by the coalescence of well-elongated α-Al_2O_3 colonies. Fig. 4 shows the TEM micrographs of α-Al_2O_3 nanofibers calcined at 1200 °C. Identical electronic diffraction (ED) patterns were taken at regions A and B (Fig. 4(a)), as well as regions C, D, E and F (Fig. 4(b)), indicating that the crystal orientations were the same throughout the sample and that the nanofibers possessed a single-crystal structure. ED patterns also revealed that the α-Al_2O_3 nanofibers grew along the [1 1 2] or [1 1 0] directions. Fig. 5 shows the ED patterns and HR-TEM images of the connection point of the square area in Fig. 4(b). All ED patterns exhibited the same zone axis. However separate spots were well documented in the ED patterns of region B. The HR-TEM images (Fig. 5(b)) confirm that there was a low-angle grain boundary in this area. Penn and Banfield[34] pointed out that crystal defects observed by HR-TEM can be attributed to the growth process when nanocrystals grow via oriented attachment. The crystal with a small misorientation in the interface is called defective single crystal.[35] The growth mechanism of coalescence is analogous to that of oriented attachment, which is a growth process describing that two or more small crystallites can merge and then rotate to form a large single crystal. In this study, low-angle grain boundary observed could be an evi-

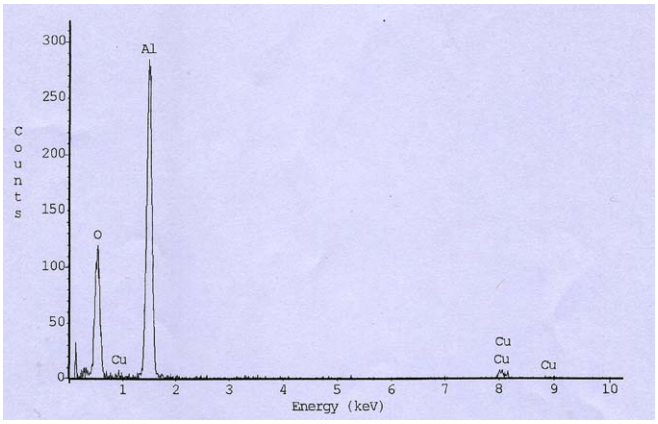

Fig. 6. EDS analysis of the nanofibers shows that only Al and O were identified.

dence that single-crystal α-Al_2O_3 nanofibers were formed by the coalescence of well-elongated α-Al_2O_3 colonies.

From the EDS analysis (Fig. 6), only Al and O were identified, meaning that the silicon wafer did not participate in the reaction. The coalescence growth of α-Al_2O_3 nanofibers behaved in a manner similar to the vermicular growth[26–30] of α-Al_2O_3 crystallites. The main difference between these two processes is that the growth of α-Al_2O_3 nanofibers is restricted by the outline of the spun fibers. Furthermore, coalescence can only occur at the ends of each elongated unit.

3.4. Thermodynamic description

The nucleation and growth mechanism has been considered as the elementary procedure for forming a new phase.[36–39] For thermodynamic consideration, the total free energy change ΔG_r for the formation of this new phase is the sum of the changes in the surface energy $S\Delta\gamma$ and volume energy $V\Delta Gv$. Based on this, the following relation applies:

$$\Delta G_r = S\Delta\gamma + V\Delta Gv \quad (1)$$

where S and V are the surface area (m^2) and volume (m^3) of the new phase, respectively. The parameters $\Delta\gamma$ and ΔGv are the differences in surface free energy (J/m^2) and volume free energy (J/m^3) between the initial phase and the new phase, respectively. During phase formation, the new phase continues growing until it exceeds the size beyond which it is thermodynamically stable. At this point, the volume energy decrease overcomes the surface energy increase, resulting in a total free energy change $\Delta G_r \leq 0$. For a spherical crystallite, Eq. (1) becomes the following expression:

$$\Delta G_r = \pi d_s^2 \Delta\gamma + \frac{1}{6}\pi d_s^3 \Delta Gv \quad (2)$$

where d_s is the diameter of the new phase. The values of the individual terms (i.e., $\pi d_s^2\Delta\gamma$ and $1/6\pi d_s^3\Delta Gv$) and the sum ΔG_r against d_s in Eq. (2) are shown in Fig. 7(a). Clearly, at the d_s value represented by point A ($\Delta G_r = 0$) and higher, beyond $\Delta G_r < 0$, the spherical crystallite is thermodynamically stable.

When the shape of the stable spherical crystallite deforms from a sphere to a fiber without changing volume, the surface

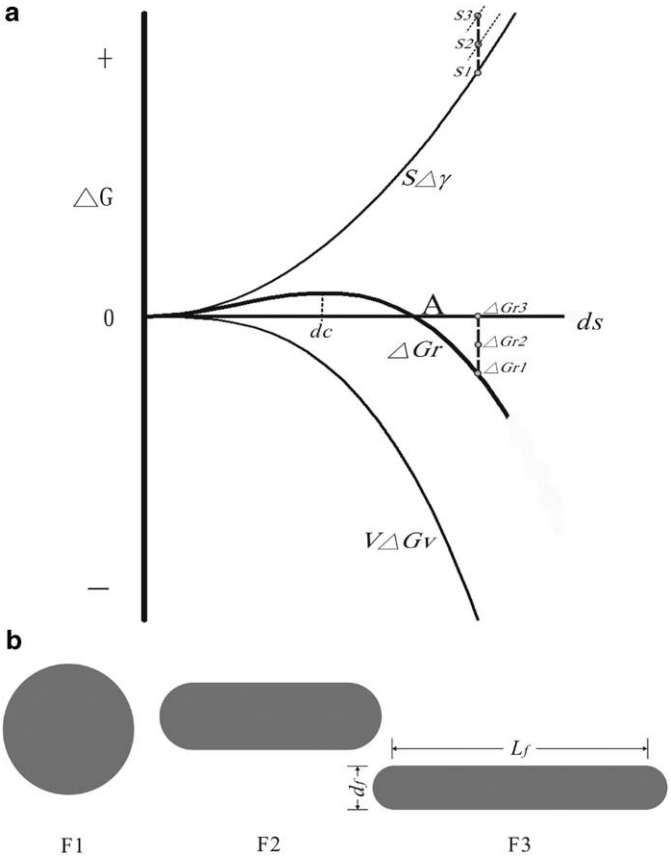

Fig. 7. The ΔG_r values increase for a spherical particle with fixed volume as the shape changes from a sphere to a fiber. ΔG_r increases from ΔG_{r1} to ΔG_{r2} and then to ΔG_{r3}, corresponding to the surface energy increases from points S_1 to S_2 and then to S_3 (a), as the shape changes from F1 to F2 and then to F3 (b).

area of the crystallite S_f will increase correspondingly. Thus, Eq. (1) becomes the following expression:

$$\Delta G_r = S_f\Delta\gamma + V_s\Delta Gv \quad (3)$$

Assuming that the ends of a fiber with length L_f are hemispherical (Fig. 7(b)), the surface area and volume V_f of the fiber can be expressed as Eqs. (4) and (5):

$$S_f = \pi d_f^2 + \pi d_f \cdot L_f > \pi d_S^2 \quad (4)$$

$$V_f = \frac{1}{6}\pi d_F^3 + \frac{1}{4}\pi d_F^2 \cdot L_f = \frac{1}{6}\pi d_s^3 \quad (5)$$

Substituting Eqs. (4) and (5) into Eq. (3), we obtain the following relation:

$$\Delta G_r = (\pi d_f^2 + \pi d_f \cdot L_f)\Delta\gamma + \left(\frac{1}{6}\pi {d_f}^3 + \frac{1}{4}\pi d_f^2 \cdot L_f\right)\Delta Gv$$

where d_f and L_f are the diameter and length of a fiber, respectively. For the fiber to be thermodynamically stable, the surface energy change of the fiber $S_f\Delta\gamma$ must be less than the volume energy change $V_f\Delta G_v$ (or $V_s\Delta G_v$). Thus, the following relationships can be expressed:

$$S_f \cdot \Delta\gamma \leq -V_s \cdot \Delta G_v \quad (6)$$

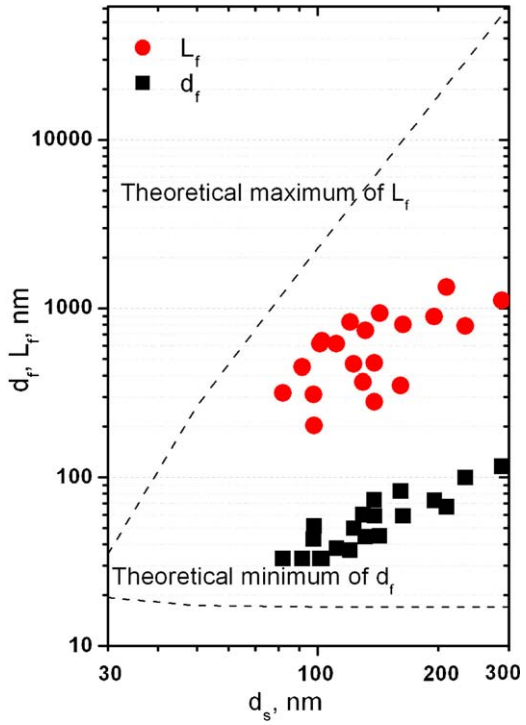

Fig. 8. The predicted ranges of d_f and L_f of α-Al_2O_3 nanofibers with the corresponding d_s of a sphere. The dashed lines represent the limits of d_f and L_f for the α-Al_2O_3 nanofibers. The symbols (■ and ●) represent the measured d_f and L_f data of coalesced α-Al_2O colonies in this study.

or:

$$(\pi d_f^2 + \pi d_f \cdot L_f)\Delta\gamma \leq -\left(\frac{1}{6}\pi d_s^3\right)\Delta G_v \quad (7)$$

From Eq. (5), the L_f expressed by d_f and d_s can be obtained as follows:

$$L_f = \frac{2}{3}\left(\frac{{d_s}^3}{{d_f}^3} - 1\right) d_f \quad (8)$$

Substituting for L_f in Eq. (7) with Eq. (8), we have the following expression:

$$2{d_f}^3 + \left(\frac{\Delta G_v}{\Delta\gamma}{d_s}^3\right) d_f + 4{d_s}^3 \leq 0 \quad (9)$$

If ΔG_v, $\Delta\gamma$, and d_s are known, the theoretical minimum value of d_f can be obtained from Eq. (9). Then, the theoretical maximum value of L_f can also be obtained from Eq. (8).

Fig. 7 depicts the increase in surface energy of a particle at a fixed volume. As the shape deforms from a sphere F1 to a slightly elongated particle F2 and then to a well-elongated fiber F3, the surface energy will increase from state S1 to S2, finally reaching state S3. Consequently, the total free energy change ΔG_r increases from state G1 to G2, finally reaching state G3.

A thermodynamic calculation of Eqs. (9) and (8) is proposed in this study using values of $\Delta\gamma$ and ΔGv that have been reported previously.[26,40,41] The surface and volume free energies of θ-Al_2O_3 are taken as 2.16 J/m^2 and -73.316×10^9 J/m^3, and those of α-Al_2O_3 are 2.64 J/m^2 and -73.429×10^9 J/m^3. Fig. 8 represents the ranges of d_f and L_f for stable α-Al_2O_3 nanofibers with the corresponding d_s value of a sphere (dashed lines). This figure also shows the values of d_f and L_f for 20 measured α-Al_2O_3 colonies that were synthesized in this study. Clearly, the values of d_f and L_f are between the two predicted limiting lines. In addition, Eq. (6), $S_f \cdot \Delta\gamma \leq -V_s \cdot \Delta G_v$, is well documented. From thermodynamic calculations, the theoretical smallest diameter of a α-Al_2O_3 nanofiber is around 17 nm.

4. Conclusions

This study examined the growth-related microstructures and the length-to-diameter ratio of single-crystal-type α-Al_2O_3 nanofibers using HR-TEM. Fibers with cross-sectional diameters of <100 nm were fabricated by an electrospinning method. The single-crystal nanofibers were found to form via the coalescence of well-elongated α-Al_2O_3 colonies. The long axis grew in the [1 1 0] or [1 1 2] directions. The length-to-diameter ratio of each colony followed the thermodynamic requirement that the surface energy must be lower than the volume energy, $S_f \cdot \Delta\gamma \leq -V_s \cdot \Delta G_v$. Thus, there exists a size ratio limit for the length and diameter of each α-Al_2O_3 colony. Thermodynamic calculations showed that the theoretical smallest diameter of a α-Al_2O_3 nanofiber is around 17 nm.

Acknowledgements

We thank Miss Liang-Chu Wang and Mr. Shu-Hau Hsu for assistance in HR-TEM and SEM operations. This study was supported by the National Science Council, ROC under Contract No. NSC 096-2917-I-006-014 and the Ministry of Economic Affairs, ROC under Contract No. 97-EC-17–A-08-S1-023.

References

1. Fisher G. Alumina as a composite material. In: Hart LD, editor. *Alumina chemicals: science and technology handbook*. Westerville, OH: American Ceramic Society; 1990. p. 353–6.
2. Cooke TF. Inorganic fibers – a literature review. *J Am Ceram Soc* 1991;**74**:2959–78.
3. Chiou YH, Tsai MT, Shih HC. The preparation of alumina fibre by sol–gel processing. *J Mater Sci* 1994;**29**:2378–88.
4. Venkatesh R, Chakrabarty PK, Siladitya B, Chatterjee M, Ganguli D. Preparation of alumina fibre mats by a sol–gel spinning technique. *Ceram Inter* 1999;**25**:539–43.
5. Venkatesh R, Ramanan SR. Influence of processing variables on the microstructure of sol–gel spun alumina fibres. *Mater Lett* 2002;**55**:189–95.
6. Chatterjee M, Naskar MK, Chakrabarty PK, Ganguli D. Sol–gel alumina fibre mats for high-temperature application. *Mater Lett* 2002;**57**:87–93.
7. Okamura K. Ceramic fibers from ceramic precursors. *Composites* 1987;**18**:107–20.
8. *Lawrence Berkeley Laboratory (LBL) internal report*; 1996.
9. Wagner RS, Ellis WC. Vapor–liquid–solid mechanism of single crystal growth. *Appl Phys Lett* 1964;**4**:89–90.
10. Valcárcel V, Souto A, Guitián F. Development of single-crystal α-Al_2O_3 fibers by vapor–liquid–solid deposition (VLS) from aluminum and powder silica. *Adv Mater* 1998;**10**:138–40.
11. Valcárcel V, Cerecedo C, Guitián F. Method for production of α-Alumina whiskers via vapor–liquid–solid deposition. *J Am Ceram Soc* 2003;**86**:1683–90.

12. Cerecedo C, Valcárcel V, Gómez M, Guitián F. Production of chromium-doped α-Al_2O_3 whiskers via vapor liquid solid deposition. *J Am Ceram Soc* 2006;**89**:323–7.
13. Cerecedo C, Valcárcel V, Gómez M, Drubi I, Guitián F. New massive vapor–liquid–solid deposition of α-Al_2O_3 fibers. *Adv Eng Mater* 2007;**9**:600–3.
14. Corrochano J, Cerecedo C, Valcárcel V, Lieblich M, Guitián F. Whiskers of Al_2O_3 as reinforcement of a powder metallurgical 6061 aluminium matrix composite. *Mater Lett* 2008;**62**:103–5.
15. Peng XS, Zhang LD, Meng GW, Wang XF, Wang YW, Wang CZ, et al. Photoluminescence and infrared properties of α-Al_2O_3 nanowires and nanobelts. *J Phys Chem B* 2002;**106**:11163–7.
16. Deng C-J, Yu P, Yau M-Y, Ku C-S, Ng, Dickon HL. Fabrication of single-crystal α-Al_2O_3 nanorods by displacement reaction. *J Am Ceram Soc* 2003;**86**:1385–8.
17. Ng, Dickon HL, Yu P, Ma NG, Lo CK, Kwok WY, Yau MY, et al. Formation of micro-sized and nanometer-sized single crystal alumina whiskers by displacement reactions. *J Eur Ceram Soc* 2006;**26**:1561–5.
18. Zhou J, Deng SZ, Chen J, She JC, Xu NS. Synthesis of crystalline alumina nanowires and nonotrees. *Chem Phys Lett* 2002;**265**:505–8.
19. Li F-Y, Qin C-D, Ng, Dickon HL. Morphology and growth mechanism of alumina whisker in aluminum-based metal matrix composites. *J Mater Res* 1999;**14**:2997–3000.
20. Sigmund W, Yuh J, Park H, Maneeratana V, Pyrgiotakis G, Daga A, et al. Processing and structure relationships in electrospinning of ceramic fiber systems. *J Am Ceram Soc* 2006;**89**:395–407.
21. Teo WE, Ramakrishna S. A review on electrospinning design and nanofiber assemblies. *Nanotechnology* 2006;**17**:R89–106.
22. Li D, Xia Y. Electrospnning of nanofibers: reinventing the wheel. *Adv Mater* 2004;**16**:1151–70.
23. Li D, McCann JT, Xia Y. Electrospinning: a simple and versatile technique for producing ceramic nanofibers and nanotubes. *J Am Ceram Soc* 2006;**89**:1861–9.
24. Azad A-M. Fabrication of transparent alumina(Al_2O_3) nanofibers by electrospinning. *Mater Sci Eng A* 2006;**435–436**:468–73.
25. Panda PK, Ramakrishna S. Electrospinning of alumina nanofibers using different precursors. *J Mater Sci* 2007;**42**:2189–93.
26. Yang RJ, Yu PC, Chen CC, Yen FS. Growth thermodynamics of nano-scaled alpha-alumina crystallites. *Cryst Grow Des* 2009;**9**:1692–7.
27. Badker PA, Bailey JE. The mechanism of simultaneous sintering and phase transformation in alumina. *J Mater Sci* 1976;**11**:1794–806.
28. Dynys FW, Halloran JW. Alpha alumina formation in alum-derived gamma alumina. *J Am Ceram Soc* 1982;**65**:442–8.
29. Hench LL, Ulrich DR. *Ultrastructure processing of ceramics, glasses and composites*. New York: John Wiley and Sons; 1984. p. 142–51.
30. Wynnyckyj JR, Morris CG. A shear-type allotropic transformation in alumina. *Metall Trans B* 1985;**16B**:345–53.
31. Cullity BD. *Elements of X-ray diffraction*. 2nd ed. London: Addison-Wesley Publishing Company, Inc.; 1978. p. 81–106.
32. Yuh J, Perez L, Sigmund WM, Nino JC. Sol–gel based synthesis of complex oxide nanofibers. *J Sol–Gel Sci Technol* 2007;**42**:323–9.
33. Wefers K, Misra C. *Alcoa technical paper no. 19*. Pittsburgh, PA: Alcoa Laboratories; 1987.
34. Penn RL, Banfield JF. Imperfect oriented attachment: dislocation generation in defect-free nanocrystals. *Science* 1998;**281**: 969–71.
35. Banfield JF, Navrotsky A. *Reviews in mineralogy and geochemistry: nanoparticles and the environment*. DC: The Mineralogical Society of America; 2001. p. 41–6.
36. Putnis A. *Introduction to mineral sciences*. New York: Cambridge University Press; 1992. p. 333–58.
37. Myerson AS, Ginde R. In: Myerson AS, editor. *Handbook of industrial crystallization*. Boston: Butterworth-Heinemann; 1993. p. 33–63 [chapter 2].
38. Kingery WD, Bowen HK, Uhlmann DR. *Introduction to ceramics*. 2nd ed. New York: John Wiley & Sons; 1976. p. 328–46.
39. Chiang YM, Birnie III D, Kingery WD. *Physical materials – principles for ceramic science and engineering*. New York: John Wiley & Sons; 1997. p. 430–64.
[40]. Chase MW, Davies Jr CA, Doweny JR, Fruip Jr, McDonalds RR, Syverud AN. *JANAF thermochemical tables*. 3rd ed. Washington, DC: Am. Chem. Soc.; 1986.
41. McHale JM, Auroux A, Perrotta AJ, Navrotsky A. Surface energies and thermodynamic phase stability in nanocrystalline aluminas. *Science* 1997;**277**:788–91.